# State-of-the-Art Methods for Brain Tissue Segmentation: A Review

Lingraj Dora, Sanjay Agrawal, Rutuparna Panda, and Ajith Abraham, *Senior Member, IEEE*

***Abstract*—Brain tissue segmentation is one of the most sought after research areas in medical image processing. It provides detailed quantitative brain analysis for accurate disease diagnosis, detection, and classification of abnormalities. It plays an essential role in discriminating healthy tissues from lesion tissues. Therefore, accurate disease diagnosis and treatment planning depend merely on the performance of the segmentation method used. In this review, we have studied the recent advances in brain tissue segmentation methods and their state-of-the-art in neuroscience research. The review also highlights the major challenges faced during tissue segmentation of the brain. An effective comparison is made among state-of-the-art brain tissue segmentation methods. Moreover, a study of some of the validation measures to evaluate different segmentation methods is also discussed. The brain tissue segmentation, content in terms of methodologies, and experiments presented in this review are encouraging enough to attract researchers working in this field.**

***Index Terms*—Brain tissue segmentation, clustering methods, feature extraction and classification-based methods, region-based methods, thresholding-based methods, validation measures.**

## I. Introduction

IMAGE SEGMENTATION plays a crucial role in medical image analysis. It extracts tissue from a brain image by partitioning it into a set of disjoint regions that have similar characteristics, such as intensity homogeneity, texture, etc. It is a commonly employed method of extracting tissues like white matter (WM), gray matter (GM), and cerebrospinal fluid (CSF) from magnetic resonance (MR) image for quantitative brain analysis. Segmentation of normal tissues from brain lesions helps to detect diseases like brain tumor, Alzheimer's disease (AD), Parkinson's disease, etc. It also helps in brain disorder identification and whole brain analysis of traumatic injury as well [1]–[4]. Brain tissue segmentation is one of the commonly used applications, which pave the way for detection of abnormalities like early tumor diagnosis, multiple sclerosis, AD, dementia, schizophrenia, etc., by accurately segmenting WM, GM, and CSF. Over the years, many popular brain tissue segmentation methods have been proposed in the literature. These methods are applied successfully for disease diagnosis and treatment planning. Nevertheless, in clinical evaluation and neuroscience research, it is considered as a major challenge because medical images suffer from many artifacts, such as intensity inhomogeneity (IIH), noise and abnormal tissues with heterogeneous signal intensities. Furthermore, the performance of brain tissue segmentation methods depends on several factors, such as location, size, shape, texture of tissues, and unclear tissue boundary, which are inherent in the modalities used for image acquisition [5]–[9].

Brain tissue segmentation methods can be broadly classified into five categories: 1) manual, 2) region-based, 3) thresholding-based, 4) clustering-based, and 5) feature extraction and classification-based. Soft computing techniques can also be incorporated in these methods. Manual segmentation is the process of manually dividing pixels having same intensity range by an expert/physician. It involves a well-experienced medical professional multidisciplinary board for decision-making. The multidisciplinary board may consist of radiologist/ anatomists/ pathologists, and trained technologists, depending on the research study, to arrive at a final decision. However, this method suffers from numerous problems occurring due to unclear boundary, poor tissue contrast, and inaccurate hand to eye coordination. Moreover, the method is subjective in the sense that segmentation results may change with experts or the same expert's view may vary with time. This classical method of pointing and labeling pixels in the same intensity range is also wearisome, time taking, and inaccurate. In addition, recently developed high-dimensional and multimodal imaging techniques make manual segmentation a challenging task for experts to extract information. To alleviate this problem, many automatic methods are suggested in the literature.

Statistical parametric mapping (SPM) is one of the most commonly employed methods for automatic brain tissue segmentation. It is a software package developed by the researchers of Wellcome Department of Imaging Neuroscience at University College London [10], [11]. Many of the automatic segmentation methods suffer from exhaustive search strategy and large

Manuscript received November 18, 2016; revised April 19, 2017 and May 12, 2017; accepted May 14, 2017. Date of publication June 14, 2017; date of current version December 29, 2017. *(Corresponding author: Rutuparna Panda.)*

L. Dora is with the Department of Electrical & Electronics Engineering, Veer Surendra Sai University of Technology, Burla 768018, India (e-mail: lingraj02uce157ster@gmail.com).

S. Agrawal and R. Panda are with the Department of Electronics and Computer Engineering, Veer Surendra Sai University of Technology, Burla 768018, India (e-mail: agrawals_72@yahoo.com; r_ppanda@yahoo.co.in).

A. Abraham is with the Machine Intelligence Research Labs (MIR Labs), Auburn, WA 98071 USA (e-mail: ajith.abraham@ieee.org).

Digital Object Identifier 10.1109/RBME.2017.2715350

computation time. To deal with the exhaustive search problems, segmentation methods incorporate optimization tools like genetic algorithm (GA), bacterial foraging optimization (BFO), particle swarm optimization (PSO), etc. In addition, evolutionary algorithms (EAs) are able to cope up with many ill-defined problems in brain tissue segmentation like multimodality, discontinuity, and noise [12]–[14].

The primary contribution of this paper is to survey the most recent segmentation algorithms for brain tissue segmentation and their state-of-the-art. This paper particularly focuses on three main aspects: recent trends in algorithms for brain tissue segmentation, their future scope to make the existing algorithms more robust, and the open problems. The study also focusses on the challenges faced by segmentation methods due to inherent problems in the modalities. The advantages and disadvantages of the studied algorithms are summed up in a table to provide a structured vision aspect. We have also presented and discussed standard validation measures used to quantify the performance of a segmentation method. Its applicability for clinical use and hardware implementation for real-time utilization is also discussed. The organization of the rest of the paper is as follows. Section II presents an overview of the various brain tissue segmentation methods. Section III presents the validation and performance indices for comparing the algorithms. Section IV presents the discussion and finally Section V is the conclusion.

## II. Brain Tissue Segmentation Methods

In this section, we have explicitly studied the state-of-the-art as well as recent advances in brain tissue segmentation methods. We have discussed segmentation methods using two-dimensional (2-D) and 3-D MRI. The brain tissue segmentation methods include standard image processing techniques like deformable models (DM) which is a contour- and shape-based method, region growing, fuzzy c-means (FCM), Gaussian mixture model (GMM), etc. Finally, the advantages and disadvantages of the studied methods are summarized in Table I.

### A. Region-Based methods

Region-based segmentation methods depend on the homogeneity of intensity in the image to detect the object boundary. Popular techniques under this method are as follows:

1) contour- and shape-based method;
2) region growing;
3) region-based level set method;
4) graph-based method (see Fig. 1).

The contour- and shape-based method uses T1-weighted MR images. The region-based level set methods and graph-based methods use T2-weighted MR images.

***1) Contour and Shape-Based Methods:*** In contour- and shape-based method, an initial contour is specified close to the desired boundary. Then, the method adjusts the contour toward the target boundary as per minimization of a predefined criterion. One of the popular contour- and shape-based method is DM. A knowledge-based segmentation method uses prior knowledge about the shape of the target object. It starts with an arbitrary initial boundary shape in the form of a curve. In general, active contours are DMs in which the contour deforms and develops toward the desired boundary. Kass *et al*. [15] proposed the first DM for detecting object boundary from an image. The deformation of the contour is controlled by minimizing an energy function. The energy function consists of internal and external energy terms. Internal energy handles the smoothness of the contour. The external energy term pushes the contour toward the desired features, such as gradient, texture, edge information, etc., in the image domain. Classical active contour methods depend on gradient information. In this method, the initial contour is located close to the boundary of the object of interest. This results in a strong external energy, which makes it possible to move the contour toward the desired object boundary. However, the method cannot handle the topological changes of the curve. In this regard, level set methods use parameterized curves to track contours and surface [3], [15]–[23]. Mesejo *et al*. [24] proposed a hybrid level set (HLS) method for segmentation of medical images. The method combines both region- and edge-based information with prior shape knowledge. In addition, GA estimates the parameters of the level set. Furthermore, scatter search derives the shape prior.

Active contours are of two types: 1) parameterized active contours (PAC) and 2) geometric/geodesic active contours (GAC). PAC characterizes a parameterized curve in a Lagrangian formulation. Explicit characterization of the curve makes user interaction and specification of a priori shape constraints simple. GACs are based on surface evolution theory and geometric flows essentially in light of Euler formulation. The method applies the gradient information to define an edge and is efficient enough to handle these curves. First, it takes a specified initial contour, which is close to the desired boundary. Second, it develops the contour toward the strongest gradient as per minimization of a boundary-based energy function. A level set of 2-D function implicitly characterizes this model, in which the number of iterations decide the stopping criteria [15]–[23].

In another aspect, DMs are of two types based on the feature of the object of interest, 1) edge-feature (EF) and 2) region-feature (RF). EFs are most often used approach for segmenting brain image into tissues such as WM, GM, and CSF for disease diagnosis. In EFs, edge-detection algorithms generate arbitrary contour lines around the target object. The object of interest is extracted by combining these contour lines using some similarity measures. However, edge detectors depend on image gradient information. Thus, the detectors are only able to detect objects defined by strong gradient function in the image domain. The performance of the above methods highly depends on the location of the initial contour, edge opening, weak edges, inhomogeneity, and noise. To overcome the above problems, researchers have incorporated expectation maximization (EM) algorithm, gradient vector flow or self-affine mapping system in the classical models. RFs depend on statistical and homogeneity property to identify the region of interest (ROI). Unlike EFs, RFs use certain region statistics to develop the curve toward ROI. However, they are unable to localize object boundaries. To overcome the problems in the RFs, researchers proposed to use a priori shape information or statistical information in the energy function [16]–[42].

TABLE I
ADVANTAGES AND DISADVANTAGES OF THE MOST COMMONLY USED BRAIN TISSUE SEGMENTATION METHODS

| Name of the method | Advantages | Disadvantages |
|---|---|---|
| Deformable model | The method produces good results, when contour is initialized close to the desired object boundary. Expansion or contraction of the contour over time is controlled by minimizing an energy function. | The performance of the method completely depends on initial contour location. Sensitive to noisy images with unclear boundary. |
| Level set | Able to control cavities, concavities, convolution, splitting, or merging. Involve simple parameter tuning. | Highly sensitive to noise, weak boundaries, low contrast between regions, false gradients, etc. Causes leakage of boundary or development of false gradient in heterogeneous regions. |
| PAC | PACs involve simple computations and are efficient models. | PACs cannot handle topological changes of the curve. |
| GAC | GACs have the capacity to handle topological changes of the curve, which makes them desirable in segmentation of complex shapes. They are capable of detecting interior contours, cups, multijunctions, and so forth. With the help of level set function. | Sensitive to initial contour location. |
| EF | Local edge information is used to deform and move the curve toward the target object boundaries. | Major drawbacks are weakly defined edges, noise, IIH, and computational complexity. Postprocessing is required to obtain hole-free objects. |
| RF | Able to suppress the problems of initialization and noise faced in EFs. | Performance degrades in the presence of IIH, noise and heterogeneous objects. |
| Region growing | Advantages of considering both visual features and spatial information. It is insensitive to changes in inner parts which results in closed regions. | Suffer from three main problems: 1) order of the pixel processing; 2) automatic selection of initial seed; 3) regions with hole and noise. Moreover, region growing fails to perform in the segmentation of multiple objects. |
| CV model | It is an effective means to overcome the limitations of edge-based methods. Able to detect interior contours and thus, could be used for medical images with weak boundaries. Piecewise smooth model could work for medical images with IIH. | Limited by images with complicated background and irregular intensity. Piecewise constant case only works with images having homogeneous regions. Nonconvex and nonunique nature of energy function often results to local minima during contour evolution. This case of convergence often leads to undesired segmentation result. |
| Graph-based | Integrate global information into local pairwise pixel similarities for efficient segmentation. | Difficult to discriminate pixels having same or minor differences between foreground and background using only statistical classification. |
| Fixed thresholding | This approach performs well for images with homogeneous intensity, high contrast, and discriminant gray values between object and background. It is used in brain tissue segmentation because of its easy implementation and computational efficiency. | A major drawback of this approach is that the correlation of pixels is not taken into account. Furthermore, they lead to misclassification of pixels due to noise, IIH, and tissues overlapping. These artifacts corrupt the histogram of the image, making segmentation using global thresholding a difficult task. |
| Adaptive thresholding | This approach is preferred when a single threshold value is unable to segment or a threshold value cannot obtain from histogram of an image. This is an efficient means of segmenting multiple objects from intensity histogram. | The performance of these methods is sensitive to the gray scale distribution, noise, multichannel images, and images with multimodal regions. |
| Hard clustering | Suitable for images with homogeneous regions. Due to less computational time, it is best suited for real-time image segmentation. | Sensitive to noise, IIH, and images with heterogeneous regions. |
| Soft clustering | As compared to hard clustering, it does not use a sharp boundary to divide the pixels into groups. It defines a membership function to cluster the pixels. | Sensitive to noise and IIH. Does not consider spatial information for clustering the pixels in the image domain. Furthermore, it generates local optimal solution due to poor initialization. |
| Mixture model | Statistically characterize an image. They are capable of handling bias field correction and spatial regularization in the local region by modeling the intensity variation of each tissue type by a Gaussian distribution. | Lack of spatial relation among neighboring pixels within a class. Often results in local optimum. |
| DWT | Able to analyze an image at various resolutions. Preserves edge sharpness. Provide valuable information about the localized frequency of a signal, useful for correct classification. | Sensitive to shifting in time, poor directionality, and lack of phase information. Usually includes dimension reduction scheme to improve performance. High computational complexity. |
| Gabor filter | Able to capture local features of the image, such as orientation, spatial frequency (scale), and localization. | Selection of scale and orientation is done on hit and trial basis. Results in a high-dimensional feature vector. Requires a large memory space. High computational complexity. |
| Statistical feature extraction methods | Consider the relationship between pixels. Capture local image properties, helpful to discriminate special structures like a brain tumor tissue from normal tissue. Less computational complexity. | Sensitive to images with heterogeneous intensities. Performance depends on a number of factors, such as location, size, shape and texture of tissues, unclear tissue boundary and noise, which are inherent in MR images. |
| KNN | It is an instance-based classifier. Capable of preserving information in the training images. Easy to implement. | For large databases, response time is very high. Sensitive to unwanted features as their contribution toward similarity leads to misclassification. |
| ANN | Popular machine learning algorithm. Organized structure of processing elements, resembled to the human brain. Able to perform well on complicated and multivariate nonlinear domain. Compared to statistical models, ANN avoids data allocation. Resistance to noise. | High computational complexity and response time. |
| SVM | Mostly preferred in high-dimensional feature space. High generalization performance. | Takes large training time. Requires large storage space. Patient-specific learning. |

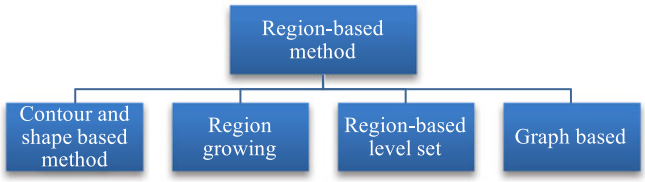


Fig. 1. Region-based methods in brain tissue segmentation.

Many techniques like region growing, region-based level set [16], [43]–[45], and graph-based methods [46], [47] overcome the limitations of the above methods by exploiting statistical estimation of regions or graph theory.

***2) Region Growing:*** Region growing method depends on the homogeneity and connectivity conditions. The classical region growing method takes a selected seed point (pixel) from each region. The surrounding pixels are collected depending upon their homogeneity criteria (e.g., intensity similarity). The process of accumulating the seed points continues until the termination condition is achieved. This results in a set of connected regions.

Region growing is a commonly practiced technique in the brain tissue segmentation. To satisfy homogeneity, it is presumed that the regions of the object of interest have same or slightly varying intensity values. Therefore, initial seed selection and different homogeneity criteria could alter the segmentation performance. For homogeneous MR images, region growing mostly produce suitable results. Furthermore, it is well suited for medical image segmentation, where images consist of mostly object and background. A possible measure to ease the problems is combining region growing method with other methods such as edge detection. Moreover, homogeneity criteria for multiple brain lesions are still to be assessed [3], [48]—[50].

***3) Region-Based Level Set Methods:*** Region-based level set methods depend on the level set to evolve the contour. The standard clustering methods like *k*-means, FCM, and GMM are used to develop the energy function of the region-based level set methods. Chan and Vese [16] proposed a region-based level set method, also called as the CV model. It is based on the idea of minimizing an energy function to deform the curve surrounding the target object. It is based on level set to develop the contour and is suited for both the piecewise constant case [16] as well as the piecewise smooth case [40]. In [16], *k*-means is employed to derive Mumford and Shah function in piecewise (PC) level set algorithm to solve two homogeneous segments. The multiphase level set algorithm uses the same concept to solve multiple segments. This approach overcomes noise and blurred boundaries. In [51] and [52], FCM and MRF are used with multiphase level set energy function to reduce the IIH effect. Furthermore, to eliminate convergence to local minima in the CV model, metaheuristic optimization algorithms are used to minimize the energy function. These types of algorithms are nongradient-type optimization and could achieve global optima. Mandal *et al*. [12] suggested a modified CV model formulated as an optimization problem. The authors used PSO to minimize the fitting energy function. This modified method is capable to achieve global minima irrespective of initial contour choice [12], [43], [53], [54].

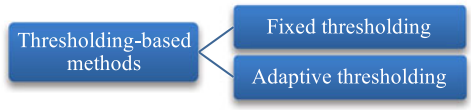


Fig. 2. Types of thresholding-based methods in brain tissue segmentation.

However, complex intensity distribution of medical images degenerates the performance of this method. In [44], estimation of phase value is overcome by using finite mixture models and GMM with the level set method. The method simultaneously estimates foreground homogeneous intensity distribution and background complex intensity distribution.

Many medical images contain complex structures. Hence, homogeneous intensity assumption for foreground is no longer valid. To improve the accuracy of the level set methods, statistical variational models like shape and additional features are utilized. For different patients, size, shape, and intensity distribution of tissues and organs would vary significantly. Consequently, it becomes a difficult task to collect training data with all types of variations. Thus, level set methods incorporating statistical prior models are limited by the segmentation accuracy [34], [55].

***4) Graph-Based Methods:*** Recently, graph-based methods are receiving attention in brain tissue segmentation. Unlike the other region-based methods, they use foreground and background seeds to locate the objects in the image. The introduction of this additional information added with local pairwise pixel similarities enhances the segmentation accuracy as compared to other methods [3]. Some of the commonly used graph-based methods are graph-cut [46], random walker (RW) [47], and geodesics shortest path [56]. Generally, medical images contain nonuniform foreground and background due to noise, complex intensity distribution, and heterogeneous intensity of abnormal tissue. In such a situation, performance of the method degrades. Recently, Li *et al*. [23] proposed a coupled statistical and graph (CSG) variational model to achieve accurate segmentation. Statistical functional estimates the multimodal intensity distribution of foreground and background. The methods also include a prior probability map to discriminate pixels with small deviations. The method is used for segmentation of tissues in computed tomography, MR images, and for tumor detection. These seed points act as hard constraints and combine global information with local pairwise pixel similarities for optimal segmentation results.

## B. Thresholding-Based Methods

Thresholding is one of the popular segmentation method, where the target objects are segmented by comparing their intensity values with one or more thresholds. It is also named as an intensity thresholding method. The threshold values can be global or local. Thresholding-based methods are of two types: 1) fixed thresholding and 2) adaptive thresholding (see Fig. 2). The thresholding-based methods use T2-weighted MR images. In fixed thresholding, pixels above the threshold level are assigned to a group and below the threshold are considered as background. However, the object of interest in MRI suffers

from many artifacts. Thus, fixed thresholding-based methods includes criterion, such as entropy, between-class variance, etc., to detect the object of interest.

If an image histogram is a bimodal pattern, then a single threshold value can separate the object from the background. It assigns intensity values above the threshold to one and below the threshold to zero, respectively. For an image $I(x, y)$, a global threshold $T$ segments the image given as

$$S(x, y) = \begin{cases} 1, & \text{if } I(x, y) \geq T \\ 0, & \text{otherwise} \end{cases} \quad (1)$$

where pixels with value 1 represents object and pixels with value 0 represents background. The segmentation accuracy of such approach highly depends on statistical fluctuations. With the increase in the number of regions, threshold selection becomes a challenging task. It may be noted that the brain tissue segmentation requires segmentation of more than two tissues (i.e., WM, GM, and CSF).

When fixed thresholding adaptively determines the threshold value for the object of interest, it is called an adaptive thresholding. In this approach, a local neighborhood surrounding a pixel adaptively determines the threshold value. Prior knowledge or local statistical properties usually estimate the threshold values. Stadlbauer *et al*. [57] used Gaussian distribution of pixel intensity levels to determine the threshold value from a T2-weighted MRI. The value determines a delineated area to identify it as a pathological tissue [57]–[59]. However, they may not perform well, when the imaging parameters use spatial information with a priori knowledge. To suppress the effect of these problems, many researchers have proposed a thresholding method based on spatial information or maximum entropy principle.

Some popular and efficient thresholding-based methods used for brain tissue segmentation of MRI are entropy-based, Otsu's method, and evolutionary-based methods. Kapur *et al*. [60] proposed maximization of entropy, to obtain the optimal threshold values from the histogram. Otsu [61] proposed a nonparametric approach called Otsu's method to find optimal threshold automatically by maximizing the between class variance of grey levels. In both the methods, computational time increases due to the extensive search strategy with the increase in the number of thresholds. Many multilevel thresholding methods are available in the literature to reduce the computational time [13], [14], [62]– [66].

Recently, EAs are used with thresholding to find the optimal threshold values efficiently by reducing the computational time. EAs are easily adaptable to ill-defined problem domain like multimodality, discontinuity, time-variance, randomness, and noise. Maitra and Chatterjee [67] used BFO in the histogram-based thresholding method for segmentation of several standard brain MRI. Manikandan *et al*. [68] obtained the optimal threshold values by maximizing the entropy using real-coded GA (RGA) with simulated binary crossover (SBX) in multilevel thresholding for segmentation of T2-weighted MRI [14], [65]–[69].

### C. Clustering Methods

In brain tissue segmentation, clustering methods are statistical techniques based on pixels. In this approach, some similarity measures, such as distance, connectivity, and intensity, divide the pixels into groups or clusters. Clustering methods are broadly of two types: 1) hard clustering and 2) soft clustering (see Fig. 3). The clustering methods use T1-weighted MR images.

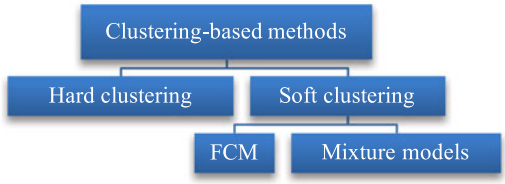


Fig. 3. Clustering methods in brain tissue segmentation.

The first approach uses crisp boundary values to divide the pixels into clusters. *k*-means is an example of hard clustering. The soft clustering is again classified into FCM and mixture models. In this approach, division of pixels is gradual, i.e., a membership function (based on FCM) or an underline probability (based on mixture models) is used to define whether a pixel belongs to a cluster or not. The membership function in FCM-based methods defines the degree by which a pixel belongs to a cluster by assigning it a membership grade value. The mixture models assume some distributional form for the underlying probability of the data to cluster it into different groups [4], [70]–[75]. A dedicated software named SPM based on the mixture models is reported in the literature for brain tissue segmentation. It can perform tasks such as skull stripping, bias field correction, and automatic segmentation. Brain tissue segmentation using SPM can be accomplished in three ways:

1) default segmentation;
2) new segmentation using SPM8;
3) modified design using hidden Markov random field (HMRF).

The SPM package has been widely adopted in the neuroimaging community for the analysis of functional and structural brain images in an automatic way. Yet, few works are described regarding the segmentation accuracy of the software as compared to other methods for segmenting GM, WM, and CSF [11]. Furthermore, a domain expert's presence may be helpful while designing any sophisticated software for improved brain tissue segmentation results.

***1) FCM:*** Among all methods, FCM is the most popular soft clustering method, which presumes that image pixels (or voxels) belong to more than one cluster. The division of pixels into clusters uses a similarity criterion. Therefore, it may not be suitable for segmenting images corrupted by noise and artifacts like IIH or shading effect in MRI. Thus, many modified FCM approaches presented in the literature help us to prepare FCM for better tissue segmentation [72]–[75].

Additionally, to suppress intensity nonuniformity (INU) effect, researchers modeled it as a multiplicative bias field (i.e., B-spline surface) and used dissimilarity index for spatial voxel connectivity. The method effectively segments brain MRI affected by noise and INU. Chuang *et al*. [75] proposed spatial FCM (sFCM), which uses a weighted membership function. The main attraction of this method is suppression of INU, elimination of noisy spots, and compression of spurious blobs. It

efficiently segments T1- and T2-weighted brain MRI scans. A way to modify sFCM is using wrapping-based curvelet mapping as a preprocessing step to remove noise in MRI. Fast spatial constraint, fuzzy kernel FCM (FKFCM) map input data (i.e., pixel intensities) to a higher dimensional space using kernel technique for clustering. FKFCM performs a satisfactory segmentation of MRI. The experiments with synthetic images, digital phantom, and clinical images affected by noise shows the strength of the method [4], [76]– [79].

Many researchers have proposed generalized FCM by modifying its objective function for robust brain tissue segmentation. Bias-corrected FCM suppresses the effect of IIH caused by bias field in the MRI. The method modifies the objective function and introduces a regularization, thereby allowing pixel labeling according to its neighborhood. It performs well for MR images corrupted with salt and pepper noise at an expense of large computational time. Alternately, for smoothness of bias field without any regularization, FCM includes a coherent local intensity clustering (CLIC) criterion. This method assumes intensity at local region to be coherent and intrinsically includes a Gaussian kernel in the energy function for bias correction. Addition of regularization further enhances the performance of this method. Some researchers used CLIC criteria to convert multiplicative bias field to an additive form of reducing complexity at the expense of partial volume effect (PVE) effect. Nonlocal regularized FCM (NLRFCM) method uses nonlocal spatial regularization to preserve the fine brain structures [72], [75], [77], [80]–[90].

Recently, Adhikari *et al*. [4] proposed a conditional spatial FCM (csFCM) method that is robust even in the presence of IIH and noise in MRI. The method considers local intensity relations between pixels to modify the membership function of standard FCM. In addition, it uses the conditioning variable related to each pixel to develop the membership functions and various clusters. Nevertheless, the presence of high levels of noise and IIH may lead to undesired segmentation. Inclusion of spatial information and IIH in the membership function of csFCM could be a relevant technique to increase its performance.

Many researchers have used EAs like PSO, a probabilistic heuristic algorithm, to initialize cluster centers in the FCM. For instance, Benaichouche *et al*. [91] used PSO to initialize cluster centers in FCM and obtained global optimum solution. In addition, it uses spatial information and Mahalanobis distance for making the method efficient against noise and misclustering. Mekhmoukh and Mokrani [92] proposed an improved kernel possibilistic *c*-means (IKPCM) based on PSO. The author used PSO for initialization of cluster centers and membership function. The method effectively segments different brain tissues.

***2) Mixture Models:*** In brain MR images, intensity values of different substructures and tissues relatively differ. In such situation, statistical mixture models are employed to characterize an image. In this approach, maximum-likelihood (ML) similarity criterion or maximum a posteriori (MAP) criterion using parametric models estimate the probability distribution of intensity in an image. GMM is a popular statistical model widely used in neuroscience. This model estimates the intensities of pixels (or voxel) in a region by a Gaussian distribution. The expectation maximization (EM) algorithm then estimates the parameters in GMM by maximizing the likelihood of the observed image.

Wells *et al*. [93] proposed an EM-based adaptive segmentation (AS-EM) algorithm for MRI. AS-EM assumed bias field to be a Gaussian distribution and modeled it by using ML. The method uses the EM algorithm to estimate the model parameters. Guillemaud and Brady [94] suggested a more generalized method, considering the limitations of [93] such as selection of number of tissue classes for modeling, parameter definitions, and spatial information about tissues. The method efficiently segments brain and breast MR images. In [95], an automatic model based on the EM (AM-EM) method estimates the bias field. The method uses digital brain atlas of MRI for grouping tissues into WM, GM, and CSF. Yet, in the above approaches, estimation of GMM parameters using EM suffers from lack of spatial information and uncertainty in segmentation. Blekas *et al*. [88] added spatial information in GMM using prior Gibbs distribution. They concluded that if the distance function becomes a discrete total variation, regularization could be introduced in the GMM. Their approach gives a spatially constrained GMM, which is immune to noise but lacks bias correction. Greenspan *et al*. [87] proposed a constrained GMM, which includes local spatial modeling with global intensity modeling. Liu and Zhang [90] proposed a local GMM, which considered both bias correction and spatial regularization. Bias correction, uses a Gaussian kernel in the objective function. Regularization of an indicator function results in smooth segmentation. However, their approach lacked in preserving the complete brain structure. Dong and Peng [96] proposed a variational model by integrating both local GMM and nonlocal spatial regularization. To ensure bias field smoothness, the authors used a truncated kernel function without additional constraints in the GMM. In addition, nonlocal spatial regularization ensured to preserve the fine details [74], [95], [97], [98].

The above EM-based ML estimation methods suffer from drawbacks like overfitting and prone to be trapped in local optima. When prior knowledge about the image is available, MAP estimation is preferred to ML. In [99], an adaptive MAP criterion estimates the model parameters. Several researchers also used MRF with parametric models for brain tissue segmentation and classification. In MRF-based approach, modeling voxel class labels as an MRF helps to estimate prior of voxel's spatial dependence. Iterated conditional modes (ICM) could be a standard solution [100]–[103]. It is a computationally efficient way, but results in local optima. Zhang *et al*. [100] proposed hidden MRF-EM method for brain image segmentation. It is a two-step iterative method. First, ICM finds the hidden class labels. Second, EM algorithm estimates the model parameters. The method provides high computational efficiency and ease of implementation. Nonetheless, both EM and ICM are deterministic searching methods, which results in local convergence. Thus, Markov chain Monte Carlo (MCMC) [104], a global statistical inference method, replaced the deterministic routines [105], [106].

Several researchers have used EAs in model-based methods like EM-based ML estimation. The aim is to overcome their inherent limitations such as overfitting and tendency of trapping in local optima. Tohka *et al*. [107] proposed a GA-EM algorithm

for likelihood estimation. As stated earlier, HMRF-EM-based methods also suffer from local convergence. Thus, the EAs substitute EM algorithm for estimating parameters. Evolutionary HMRF method uses EAs such as clonal selection algorithm (CSA) to estimate the parameters of HMRF. The method is well suited for segmentation of both simulated and real brain MR images. Recently, a HMRF-CSA algorithm combines both CSA and MCMC to improve the performance of the HMRF technique. To demonstrate the performance of the method, clinical brain images are used for segmentation [108], [107], [109], [110].

### D. Feature Extraction and Classification-Based Methods

Feature extraction and classification methods play a vital role in brain tissue segmentation. It uses T2-weighted MR images. In this method, the primary task is to obtain a set of most effective and discriminating features from the MR brain image. The discriminating features are then used for classification. Many state-of-the-art feature extraction methods such as discrete wavelet transform (DWT) [111], Gabor filter, and statistical methods like gray level co-occurrence matrix, gray level run length matrix, etc., [112] are reported in the literature. However, feature extraction from MR images remains a challenging task due to artifacts like noise, IIH, etc. In addition, high dimensionality is an inherent problem with most of the feature extraction methods. Principal component analysis (PCA), linear discriminant analysis (LDA), etc., solves the dimensionality problem to some extent. They obtain a small set of significant features for correct classification.

State-of-the-art classification methods are k-nearest neighbors (KNN), support vector machine (SVM), artificial neural network (ANN), self-organizing map, etc. The detail description about their advantages and disadvantages is given in [113].

In most of the above-cited methods, the training process of a classifier does not affect the nature of the extracted features. In addition, most of the feature extraction methods require spatial and intensity information for accurate segmentation. Recently, convolutional neural networks (CNNs) and deep learning are gaining recognition in brain tissue segmentation [114]–[117]. Unlike classical feature extraction and classification-based methods, they avoid the explicit requirement of the spatial and intensity information. CNNs learn from a set of convolutional kernels. The convolutional kernels are explicitly trained for a desired classification. In addition, CNNs optimize the kernels based on the input training information. Furthermore, the spatial and intensity information can also be incorporated in order to differentiate between classes. In [117], a CNN-based method is proposed using MRI of infants. The authors used T1-weighted, T2-weighted, and fractional anisotropy images for segmentation of three tissues: WM, GM, and CSF. In [116], the authors present a method for tissue segmentation of adults using T1-weighted MRI, as part of the medical image computing and computer-assisted intervention (MICCAI) challenge on multi-atlas labeling. The methods in [116] and [117] utilize CNNs but lacks intensity and spatial properties. Moeskops *et al*. [114] proposed a CNN-based method that employs multiple patch sizes as well as multiple convolution kernel sizes to retain multiscale features. This learning scheme allows to approximate both spatial and intensity properties for accurate segmentation of MRI into various tissue classes.

The advantages and disadvantages of the most commonly used brain tissue segmentation methods are illustrated in Table I.

## III. Validation Measures

In this paper, we have presented some of the state-of-the-art validation measures used for brain tissue segmentation. Validation of segmentation method is a necessary measure to quantify its performance and limitations. Moreover, it is also preferred before applying a method for clinical usage. However, validation of a method requires data to evaluate its performance. In brain tissue segmentation, data is a medical brain image, which is of two types: synthetic image and real image. Here, we discuss about synthetic and real clinical images. Later, we have also presented some of the popular publicly available databases used in the validation of a segmentation method.

### A. Synthetic Image

Synthetic images are developed using a computer without a real scanner. The advantage is that user can define the parameters to generate a desired image. For instance, by defining different MR parameter values like echo time (TE), repetition time (TR), resolution, sequence, noise, and IIH, three types of MR images are generated: T1-weighted (T1-w), T2-weighted (T2-w), and proton density weighted. In addition, ground truth image is also available to compare the efficiency of the segmentation result. An MRI simulator can generate synthetic image of various complexity levels from piecewise constant image to realistic image.

Several researchers have used synthetic brain MR images generated from simulator to evaluate their segmentation method. Evaluation using synthetic images is the most common approach because of its ease. In addition, synthetic images generated by the MR simulator could be a good choice for comparing different techniques. However, it is not possible to generate perfect real images from the MR simulator. Phantoms can be utilized to generate real images, but it is difficult to have dense ground truth for phantom images [118].

### B. Clinical Image

Validating segmentation methods using real clinical images are an essential step to measure the effectiveness of the methods. While using a real clinical database, we must take care about the heterogeneity of the disease. For this reason, data are taken from enough patients. Another aspect is the unavailability of the ground truth image. Although it plays a vital role to measure the performance of segmentation, it is not essential to measure the reproducibility of a method. Oftentimes the results of automatic segmentation methods are compared with manual segmentation carried out by an expert. Nevertheless, a well-known error called inter- and intraexpert variability puts limits to manual segmentation.

### C. Databases

Some of the publicly available standard databases used for quantitative evaluation of brain tissue segmentation methods

TABLE II
COMMONLY USED DATABASES IN BRAIN TISSUE SEGMENTATION

| Name of the database | Types of image available | Download link |
|---|---|---|
| BrainWeb | Simulated brain MR images generated by using three sequences (T1-, T2-, and proton-density(PD)-weighted) along with a variety of slice thicknesses, noise levels, and intensity inhomogeneity levels | http://brainweb.bic.mni.mcgill.ca/brainweb/ |
| IBSR | Provides MRI along with manually segmented images for comparing automatic segmentation results | https://www.nitrc.org/projects/ibsr |
| Harvard medical school website | It is a database which contains various types of images like normal brain images, images for cerebrovascular diseases, brain tumor images, degenerative diseases images, inflammatory or infectious diseases images | http://www.med.harvard.edu/aanlib/home.htm |
| Allen brain atlas | Allen human brain atlas, Brainspan atlas of the developing human brain, Aging, dementia and traumatic brain injury, Allen spinal cord atlas | http://www.brain-map.org/ |
| Medical image computing and computer assisted intervention | Multicontrast MR scans | http://martinos.org/qtim/miccai2013/data.html |
| The Cancer Imaging Archive (TCIA) | Contains medical images of subjects having cancer and/or anatomical site like lung, brain, etc. | http://www.cancerimagingarchive.net/ |


Fig. 4. Example simulated T1-w MR image of a subject from BrainWeb. (a) Normal MRI. (b) Segmented WM. (c) Segmented GM. (d) Segmented CSF.


Fig. 5. Example of MRI from Allen brain atlas. (a) T1-w MRI. (b) T2-w MRI.

are described in Table II. An instance of simulated T1-w MR image of a subject from BrainWeb is shown in Fig. 4. The image [see Fig. 4(a)] is about 362 × 362 pixels. Ground truth images of the tissues: WM [see Fig. 4(b)], GM [see Fig. 4(c)], and CSF [see Fig. 4(d)] is also available in the database.

The Allen brain database also contains MR images (see Fig. 5). Likewise, the above available databases, researchers also obtained medical brain images from hospitals or by direct scanning. Most of the time, real clinical images are used to check the strength of the proposed segmentation method for clinical use. Mostly, methods are first checked with simulated data and then with real data.

### D. Performance Indices

Performance indices are used to validate a segmentation method. Validation of a method is a necessary step before it is applied for clinical evaluation. In this section, we have presented various performance indices used to evaluate brain tissue segmentation methods. No single index is used to judge the performance of the segmentation methods. In brain tissue segmentation, different measures used for quantitative evaluation of methods are given as follows:

*Dice index (DI):* It is a quantitative overlap measure used to evaluate the segmentation methods. DI is calculated for each tissue type, dataset, and method. It measures the amount of overlap between the segmented image and the ground truth image. It is defined as [4]

$$\mathrm{DI} = \frac{2V_{ae}}{V_a + V_e}. \tag{2}$$

*Partition coefficient:* Partition coefficient ($V_{\mathrm{pc}}$) is a significant indicator of fuzzy partition. Its value ranges between 0 and 1, with 1 as its optimal value. Higher value represents better performance with less fuzziness. It is given as

$$V_{\mathrm{pc}} = \frac{1}{N}\sum_{i=1}^{C}\sum_{j=1}^{N} z_{ij}^2 \tag{3}$$

where $z_{ij}$ is the weighted membership variable, $C$ is the number of clusters, and $N$ is the number of data patterns [4].

*Partition entropy* ($V_{\mathrm{pe}}$)*:* Partition entropy is another measure to indicate fuzzy partition. The minimum value of $V_{\mathrm{pe}}$ indicates a best clustering. The optimal value of $V_{\mathrm{pe}}$ is 0. It is given as [4]

$$V_{\mathrm{pe}} = \frac{1}{N}\sum_{i=1}^{C}\sum_{j=1}^{N} z_{ij}\log z_{ij}. \tag{4}$$

*Jaccard index (JI):* JI is also a measure of overlap between the segmented image and the ground image. If JI is 0, it implies no overlap with ground truth and a value of 1 implies perfect segmentation

$$\mathrm{JI} = \frac{|S \cap G|}{|S \cup G|} \tag{5}$$

where $S$ and $G$ are two segments generated by the method and ground truth [92].

*Similarity index($\rho$):* Similarity index is used for comparison between the segmented image and the ground truth image. It is defined as

$$\rho = \frac{1}{C}\sum_{i=1}^{C}\frac{2\left|A_i \cap B_i\right|}{\left|A_i\right| + \left|B_i\right|} \tag{6}$$

where $A_i$ is the number of pixels belonging to cluster $C_i$ obtained from segmentation and $B_i$ is the number of pixels in $C_i$ as per ground truth. A range of $\rho$ is [0, 1], and $\rho = 1$ is its optimal value [4].

*Segmentation accuracy (SA):* Segmentation accuracy is the sum of correctly classified pixels divided by the total number of pixels in the clustered image. It is given as

$$\mathrm{SA} = \frac{\sum_{k=1}^{M}\mathrm{card}\left(A_k \cap C_k\right)}{\sum_{k=1}^{M}\mathrm{card}\left(C_k\right)} \tag{7}$$

where $M$ is the total number of pixels in a cluster, $A_k$ is the number pixels belonging to the $k$th cluster obtained from segmentation, and $C_k$ is the number of pixels in the $k$th cluster in ground image. The optimal value of SA is 1 [4].

*Tissue segmentation accuracy (TSA):* It is defined as

$$\mathrm{TSA} = \frac{2N_{\mathrm{CTK}}}{N_{\mathrm{CITK}} + N_{\mathrm{GTK}}} \tag{8}$$

where $N_{\mathrm{CTK}}$ is the number of pixels that are correctly (inside the mask of ground truth) assigned to tissue $k$ by a given method. $N_{\mathrm{CITK}}$ is the total number of pixels (inside and outside the mask of ground truth) assigned to tissue $k$. $N_{\mathrm{GTK}}$ is the number of pixels belonging to tissue $k$ in the discrete anatomical model (the ground truth mask). For ideal segmentation, the optimal value of TSA is 1 [4].

*Uniformity measure (UM):* It is a quantitative validation to measure the efficiency of the segmentation methods. It is defined as

$$\mathrm{UM} = 1 - 2 \times p \times \frac{\sum_{j=0}^{p}\sum_{j\in R_j}\left(f_i - \mu_j\right)^2}{N \times \left(f_{\max} - f_{\min}\right)^2} \tag{9}$$

where $p$ is the number of thresholds, $R_j$ is the $j$th segmented region, $N$ is the total number of pixels in the image, $f_i$ is the gray level of pixel $I$, $\mu_{\mathrm{j}}$ is the mean value of pixels in the $j$th region, $f_{\max}$ is the maximum gray level of pixels in the image, and $f_{\min}$ is the minimum gray level of pixels in the image. The optimal value of UM is 1 [68].

*False positive (FP) and false negative (FN):* It represents the amount of misclassification during segmentation. Besides, FPs and FNs, true positives (TPs), and true negatives (TNs) are also used. TPs and TNs represent the correct segmentation. In binary segmentation, sensitivity and specificity measures are used to evaluate the influence of FPs and FNs on the performance of a method

$$\text{sensitivity} = \frac{\mathrm{TP}}{\mathrm{TP}} + \mathrm{FN} \tag{10}$$

$$\text{specificity} = \frac{\mathrm{TN}}{\mathrm{TN}} + \mathrm{FP}. \tag{11}$$

The optimal value of the above two measures is 1 [112].

## IV. Discussion

Segmentation of brain tissues like WM, GM, and CSF is a challenging task due to IIH, noise, and other artifacts. Several methods are proposed in the literature for brain tissue segmentation, as discussed in Section II. Comparison of all these methods is quite a difficult and tedious task, as they use a different database, image modality, segmentation analysis, and validation measures. For instance, international symposium on biomedical imaging and MICCAI conduct competition in medical image processing as a part of their conference. They allow unbiased validation of several algorithms using the same database. For instance, MRBrains 2013 from MICCAI is an open challenge with 37 ranked works as of now [119]. In this challenge, researchers around the world participated to validate their methods for the segmentation of brain tissues (WM, GM, and CSF) on multisequence, such as T1-w, T2-w, inversion recovery, and fluid attenuated inversion recovery (FLAIR). All the methods are ranked using the performance indices DI, modified Hausdorff distance, and absolute volume difference on 15 test datasets. From MRBrains 2013 challenge, it is witnessed that the 3-D deep learning method (*voxnet1*) outperformed all other methods in terms of overall segmentation result and WM segmentation. The 3-D deep learning method (*voxnet2*) outperformed all other methods in terms of GM segmentation. PyraMid-long short-term memory methods achieved rank 1 in CSF segmentation. ISI-Neonatology showed better results in case of WM and GM combined segmentation. Multidimensional gated recurrent units demonstrated promising results on intracranial cavity segmentation.

In this review, we have presented a quantitative comparison of some of the state-of-the-art techniques in brain tissue segmentation. These comparisons could provide the researchers a comprehensive idea about the methods to be used in different applications. It is observed from the study that thresholding-based approaches are particularly simple and fast, when suitable threshold values are available. These approaches are used as a preprocessing step in brain tissue segmentation. Clustering-based methods like FCM are the most widely preferred approach in tissue segmentation. However, severe noise and IIH could degrade their performance noticeably. Several modified FCM techniques incorporating spatial information are reported to reduce the effect of noise and IIH during tissue segmentation. Nevertheless, clustering-based methods are time consuming during training and labeling of the data.

The region-based methods are mostly used for refinement stage in tissue segmentation. They only require an initial single seed to detect the object of interest. However, its performance depends on tissue boundary and choice of initial seed.

In brain tissue segmentation methods, use of some preprocessing steps like bias field and IIH correction, etc., can improve their performance. For instance, software package like SPM includes such preprocessing steps. Thus, using SPM for bias correction may improve their performance. In this regard, mixture models could be a better choice. They use statistical techniques to estimate and model the bias field.

### A. Quantitative Comparison

The similarity evaluation based on dice similarity coefficient (DSC) and JI using different region-based methods on T1-w MR

TABLE III
COMPARISON OF DSC AND JI WITH REGION-BASED METHODS USING T1-W MR IMAGES FROM NMR DATABASE [24]

| Name of the method | Validation measure DSC | | | Validation measure JI | | |
|---|---|---|---|---|---|---|
| | Mean | Median | Std. dev. | Mean | Median | Std. dev. |
| HLS | **0.758** | 0.780 | 0.048 | **0.612** | 0.639 | 0.062 |
| DM | 0.752 | 0.783 | 0.056 | 0.606 | 0.643 | 0.071 |
| GAC | 0.124 | 0.139 | 0.035 | 0.066 | 0.074 | 0.020 |
| DM + GAC | 0.585 | 0.613 | 0.087 | 0.418 | 0.442 | 0.084 |

Bold values indicate best results.

TABLE IV
COMPARISON OF MEAN DSC AND STD. DEV DSC WITH REGION-BASED METHODS USING T2-W MR IMAGES FROM TCIA DATABASE [23]

| Name of the method | Validation measure DSC | |
|---|---|---|
| | Mean | Std. dev. |
| CSG | **0.901** | **0.033** |
| RW | 0.814 | 0.085 |
| CV | 0.502 | 0.156 |

Bold values indicate best results.

images is illustrated in Table III. From the table, it is revealed that the HLS method outperforms all other region-based methods in terms of high mean DSC and JI. This improvement in result may be due to the use of EA like GA to produce the shape prior. In addition, GA is used to estimate the optimum learning parameters. Furthermore, it does not require any training set of images to obtain the shape of the object of interest. Hence, HLS can be a good choice for automatic segmentation.

A comparison of mean and std. dev. DSC using different region-based methods on T2-w MR images is illustrated in Table IV. From the table, it is observed that the CSG method achieved a preferably high mean DSC value and a low std. dev. DSC as compared to the other region-based methods. The reason may be that the CSG model is able to optimize the statistical intensity function using a prior probability map. Hence, it can be used for segmentation of medical images with multimodal intensity distribution, noise, and unclear boundaries.

The accuracy of FCM-based segmentation methods to extract brain tissue like WM, GM, and CSF from simulated and real T1-w MR images using DI measure is shown in Table V. From the table, we can observe that IKPCM is capable of segmenting brain tissues with a high DI for simulated MR images. Note that a high DI value is obtained from real MR images as well. The reason may be the incorporation of spatial information resulting in better extraction of tissues.

A comparison of mixture models to extract brain tissue like WM, GM, and CSF from simulated and real T1-w MR images using DI measure is presented in Table VI. It is observed that the variational method achieves a higher DI, in the presence of noise and IIH. It achieves a high DI for real MR images also. The variational method incorporates a bias field correction and spatial information. In addition, they have the capability to suppress the effect of IIH.

The accuracy of brain tissue segmentation methods using mean JI and std. dev. JI on T1-w MR images is presented in Table VII. Among the soft clustering-based methods, robust sFCM (RSFCM) method outperforms other methods with a high JI and a low std. dev JI on real MR images. It includes spatial and bias field information, which makes it robust for brain tissue segmentation.

A comparison is made considering four types of clustering methods: csFCM, sFCM, FCM, and *k*-means, based on average

TABLE V
COMPARISON OF FCM-BASED METHODS USING DI ON SIMULATED AND REAL T1-W MR IMAGES FROM BRAINWEB AND IBSR DATABASES [92]

| Method | Tissue | DI |
|---|---|---|
| IKPCM | WM (simulated) | **0.9771** |
| | GM (simulated) | **0.9761** |
| | WM (real) | **0.9791** |
| | GM (real) | **0.9783** |
| FCM + Spatial constraint | WM (simulated) | 0.9035 |
| | GM (simulated) | 0.8857 |
| | WM (real) | 0.9147 |
| | GM (real) | 0.8728 |
| FCM | WM (simulated) | 0.8671 |
| | GM (simulated) | 0.8588 |
| | WM (real) | 0.8562 |
| | GM (real) | 0.8591 |

Bold values indicate best results.

TABLE VI
COMPARISON OF MIXTURE MODEL-BASED METHODS USING DI ON SIMULATED AND REAL T1-W MR IMAGES FROM IBSR DATABASE [96]

| Method | Tissue | DI |
|---|---|---|
| Variational method | CSF (simulated) 3% noise + 20% IIH | **0.9621** |
| | WM (simulated) 3% noise + 20% IIH | **0.9782** |
| | GM (simulated) 3% noise + 20% IIH | **0.9389** |
| | WM (real) | **0.8879** |
| | GM (real) | **0.8298** |
| Local GMM | CSF (simulated) 3% noise + 20% IIH | 0.959 |
| | WM (simulated) 3% noise + 20% IIH | 0.9687 |
| | GM (simulated) 3% noise + 20% IIH | 0.9234 |
| | WM (real) | 0.8609 |
| | GM (real) | 0.8244 |
| NLRFCM | CSF (simulated) 3% noise + 20% IIH | 0.9618 |
| | WM (simulated) 3% noise + 20% IIH | 0.9762 |
| | GM (simulated) 3% noise + 20% IIH | 0.9346 |
| | WM (real) | 0.8851 |
| | GM (real) | 0.7847 |

Bold values indicate best results.

TABLE VII
COMPARISON OF SOFT CLUSTERING-BASED METHODS USING MEAN JI AND STD. DEV. JI ON T1-W MR IMAGES FROM IBSR DATABASE [97]

| Name of the method | Tissue | Validation measure JI | |
|---|---|---|---|
| | | Mean | Std. dev. |
| RSFCM | GM (real) | **0.8478** | **0.0180** |
| | WM (real) | **0.7834** | **0.0141** |
| FCM + GMM | GM (real) | 0.5930 | 0.0543 |
| | WM (real) | 0.6433 | 0.0785 |
| CLIC | GM (real) | 0.5343 | 0.0143 |
| | WM (real) | 0.6960 | 0.0702 |
| AM-EM | GM (real) | 0.7222 | 0.0800 |
| | WM (real) | 0.6213 | 0.0500 |
| AS-EM | GM (real) | 0.6239 | 0.0804 |
| | WM (real) | 0.6770 | 0.1095 |

Bold values indicate best results.

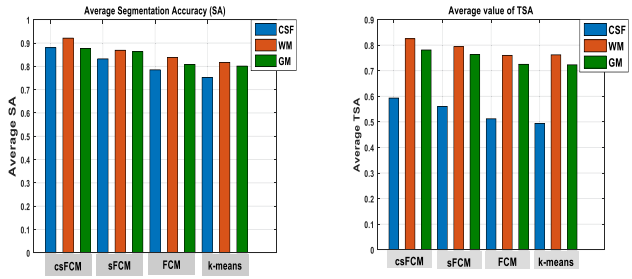


Fig. 6. (a) Comparison of average SA for segmented CSF, WM, and GM using csFCM, sFCM, FCM, and *k*-means methods on simulated T1-w MR images from Brainweb [4]. (b) Comparison of average TSA for segmented CSF, WM, and GM using of csFCM, sFCM, FCM, and *k*-means methods on simulated T1-w MR images from Brainweb [4].

TABLE VIII
COMPARISON OF SOFT CLUSTERING-BASED TISSUE SEGMENTATION METHODS USING PARTITION COEFFICIENT ($V_{\mathrm{pc}}$), PARTITION ENTROPY ($V_{\mathrm{pe}}$), AND SIMILARITY INDEX ($\rho$) USING T1-W MR IMAGES FROM BRAINWEB [4], [92]

| Method | Modality | $V_{\mathrm{pc}}$ | $V_{\mathrm{pe}}$ | $\rho$ |
|---|---|---|---|---|
| csFCM | MRI (simulated) | 0.943 | 0.096 | **76.67** |
| sFCM | MRI (simulated) | 0.897 | 0.180 | 74.351 |
| FCM | MRI (simulated) | 0.803 | 0.378 | 71.176 |
| csFCM | MRI (real) | **0.960** | **0.064** | – |
| sFCM | MRI (real) | 0.892 | 0.186 | – |
| FCM | MRI (real) | 0.803 | 0.373 | – |
| FCM + spatial constraint | MRI (simulated) | 0.8859 | 0.2831 | – |
| IKPCM | MRI (simulated) | **0.9645** | **0.0876** | – |

Bold values indicate best results.

SA [see Fig. 6(a)]. All the methods are evaluated on simulated T1-w MR images. The figure reveals that *k*-means method gives low average SA values for all types of tissues as compared to other three methods.

Similarly, the *k*-means method gives low average TSA values for CSF, WM, and GM [see Fig. 6(b)]. Thus, hard clustering method is less preferred to segment tissues of MR images with noise and heterogeneous intensity levels. Among the soft clustering methods, csFCM outperforms other two methods with high average SA values for CSF, WM, and GM [see Fig. 6(a)]. Similarly, csFCM also achieves a high average TSA value for CSF, WM, and GM [see Fig. 6(b)].

Therefore, the performance of the classical FCM method is improved by incorporating conditioning effect and spatial information into the membership function of FCM. These modifications in classical FCM make it robust against moderate noise and IIH level. However, it is sensitive to high levels of noise and IIH.

A comparison among different types of soft clustering methods: csFCM, IKPCM, sFCM, FCM plus spatial constraint, and FCM from simulated and real T1-w MRI is illustrated in Table VIII. All these methods are compared based on the partition coefficient ($V_{\mathrm{pc}}$), partition entropy ($V_{\mathrm{pe}}$), and similarity index ($\rho$). From the table, it is observed that IKPCM and csFCM achieved a better tissue segmentation having a high *Vpc* for simulated and real T1-w MR images. Furthermore, IKPCM and csFCM have a low $V_{\mathrm{pe}}$ value, which reveals better segmentation. As compared to sFCM and FCM, csFCM achieved a better tissue segmentation with a high similarity index.

TABLE IX
COMPARISON OF MIXTURE MODEL-BASED METHODS WITH AVERAGE VOXEL CLASSIFICATION ACCURACY USING REAL T1-W MR IMAGES FROM IBSR DATABASE [108]

| Modality/Tissue | FSL | SPM | GA-EM | HMRF-CSA |
|---|---|---|---|---|
| MRI | 0.7506 | 0.8120 | 0.7497 | **0.8295** |
| GM | 0.7735 | 0.8442 | 0.7790 | **0.8492** |
| WM | 0.8708 | **0.8738** | 0.8723 | 0.8388 |
| CSF | 0.1619 | 0.2031 | 0.1490 | **0.5545** |

Bold values indicate best results.

TABLE X
COMPARISON OF FEATURE EXTRACTION AND CLASSIFICATION-BASED METHODS ON T2-W PATHOLOGICAL BRAIN MR IMAGES FROM HARVARD MEDICAL SCHOOL [120]

| Method | Sensitivity | Specificity |
|---|---|---|
| DWT + PCA + BPNN | **100%** | **100%** |
| DWT + PCA + KNN | 96% | 97% |
| DWT + PCA + ANN | 95.9% | 96% |
| CAD system (FPCNN + DWT + PCA + BPNN) | **100%** | 92.8% |
| Statistical features + SVM | 96.2% | 95.7% |
| Gabor filter + SVM | 95.4% | 93.9% |

Bold values indicate best results.

A comparison of average voxel classification accuracy, using mixture models like HMRF-CSA, GA-EM algorithm, the MR image segmentation evaluation in the SPM, and the FMRIB software library (FSL) packages is presented in Table IX. From the table, it is observed that HMRF-CSA achieves a high classification accuracy as compared to other methods. The method achieves an improved accuracy, especially for GM and CSF delineation. This improvement in the result may be due to the incorporation of CSA and MCMC method for parameter estimation into the HMRF model. Hence, mixture model with global optimization technique to estimate its statistical parameters can be used for robust segmentation.

A quantitative analysis of different feature extraction and classification-based methods on pathological brain for tissue segmentation is presented in Table X. In the table, sensitivity and specificity measures are used to compare the methods and an attempt is made to compare some of the feature extraction methods, such as DWT, Gabor filter, and statistical feature extraction method. A detailed analysis of feature extraction and classification methods on pathological brain images can be found in [120].

In practice, DWT uses PCA to resolve dimensionality issue. In addition, DWT uses popular techniques such as back propagation neural network (BPNN), KNN, and ANN for classification. The other two methods use SVM for classification purpose. In addition, a computer-aided diagnosis (CAD) system is also considered for comparison. The CAD system integrates feedback pulse-coupled neural network (FPCNN) for segmentation, DWT for feature extraction, PCA for dimension reduction, and BPNN for classification of pathological T2-w MR images. From the table, it is observed that DWT + PCA + BPNN and CAD system achieved a high sensitivity. Furthermore, DWT + PCA + BPNN achieved a high specificity. A 100% sensitivity indicates FN = 0. Similarly, 100% specificity indicates FP = 0. Hence, DWT +

TABLE XI
COMPARISON OF THRESHOLDING-BASED TISSUE SEGMENTATION METHODS USING T2-W MR IMAGES FROM HARVARD MEDICAL SCHOOL [13]

| Method | Slice No. | Number of threshold | | Std. dev. | | UM | |
|---|---|---|---|---|---|---|---|
| | | 2 | 5 | 2 | 5 | 2 | 5 |
| PSO | 22 | 97, 184 | 76, 119, 154, 184, 214 | 5.9887e–04 | 0.6701 | 0.9552 | 0.9435 |
| | 32 | 107,185 | 80,112,139, 186,213 | 0.0016 | 0.9830 | 0.9368 | 0.9422 |
| BFO | 22 | 96, 184 | 44, 90, 127, 170, 208 | 2.5901e–04 | 0.0236 | 0.9569 | 0.9786 |
| | 32 | 107,185 | 80,112,139, 186,213 | 3.3569e–04 | 0.0749 | 0.9342 | 0.9668 |
| ABF | 22 | 95, 184 | 43, 88, 130, 176, 208 | 1.1721e–04 | 0.0197 | 0.9569 | 0.9785 |
| | 32 | 110,185 | 52,87,128, 167,198 | 1.0022e–04 | 0.0341 | 0.9342 | 0.9767 |
| RGA + SBX | 22 | **96, 184** | **44, 86, 127, 174, 208** | **1.9638e–14** | **8.1236e–04** | **0.9569** | **0.9788** |
| | 32 | **109,185** | **34,78,123,174,207** | **1.2497e–14** | **0.0096** | **0.9342** | **0.9843** |

Bold values indicate best results.

PCA + BPNN outperforms all other methods. Therefore, we can conclude that feature extraction and classification-based methods are well suited for tissue segmentation of pathological brain images. However, in pathological brain MR image, the complicated structure of various tissues makes it a challenging task.

Different EAs used to optimize the parameters of Kapur's entropy-based thresholding methods and Otsu method are compared in Table XI. The table shows optimum threshold values, standard deviation, and UM. From the table, it is revealed that RGA with SBX is capable of producing the global optimum solutions giving better segmentation results.

### B. Clinical Usage

From the review of the state-of-the-art brain tissue segmentation methods, it appears that researchers are advancing to develop fully automatic methods, which are clinically more feasible. This can be achieved by incorporating human intelligence, prior knowledge, and tissue information within the algorithm for robust segmentation results. Furthermore, automatic segmentation methods are desirable which are independent of patient-specific training. As far as research direction is concerned, a specific tissue segmentation method can be chosen for a particular type of diagnosis. For instance, in tissue segmentation, feature extraction and classification-based approaches are preferred when manual segmentation results are available. When multiple lesions are to be segmented, then graph-based and region-based approaches are preferred because they are more automatic, converge rapidly, and gives accurate results. When lesions are spherical or near spherical, thresholding-based methods are capable enough to produce satisfactory results with less statistical discrimination.

As far as MRI modalities are concerned, T1-w scans are capable of clearly separating GM and WM. Thus, it is preferred for intertissue classification during clinical usage. In this aspect, T2-w images are used for intratissue classification of abnormal fluid from normal tissue. Thus, for clinical usage they are well suited for brain tissue segmentation. Nowadays, many more advanced imaging techniques are being used in clinical usage, such as FLAIR, diffusion weighted imaging, etc., for efficient brain tissue segmentation. Detailed analysis of these techniques is out of the scope of this paper.

Research in brain tissue segmentation will continue to find a unified optimal solution for clinical use based on accuracy and efficiency. Indeed, the boundless solution space of segmentation encourages researchers to develop domain specific methods starting from a common solution. Improvement in segmentation methods relevant to a specific domain in brain imaging will be a new direction to handle large amount of data with less computation time.

### C. Hardware Implementation

Brain tissue segmentation using MRI is a key method for disease diagnosis, treatment planning, and guidance. Special attention is required for hardware implementation for real-time use because most of the methods suffer from high computational complexity. At the same time, medical imaging data are growing at a fast rate. In the level set method, a 2-D function implicitly defines the boundary of the object of interest. The function depends on different characteristics of the MRI. Thus, hardware implementation of the level set method using parallel processing in the spatial domain requires many interpolation operations in a single iteration. A way is to process elements in a narrow band. However, the changing nature of the narrow band demands uneven memory accesses.

The key difference between active contours and level set is that nodes instead of a function explicitly represent contours. The nodes move within the MR images to detect the tissue boundary. Normally, this process is time consuming. However, hardware implementation with parallel processing can significantly decrease the segmentation time.

Brain tissue segmentation for real-time application using region growing can be accelerated by parallel processing of many seeds with shared memory. The shared memory scheme avoids reading of same seed multiple times from global memory. However, the approach requires regular supervision, such that different regions do not access a neighbor pixel at the same time. In soft clustering-based methods like FCM, the use of Euclidean distance during membership function evaluation introduces a huge amount of complexity in hardware implementation. In addition, for a large dataset, the method requires notable time, limiting its applicability. Thus, real-time application of classical FCM is a tedious task. For hardware implementation, a way is to modify FCM keeping in view the hardware resource minimization.

In thresholding-based methods, each pixel is classified irrespective of all other pixels. In this regard, the method completely

agrees with parallel processing. In addition, the method does not require any synchronization. Furthermore, memory usage is also low. However, if we want to store the segmentation results, then the memory usage is equal to the size of the input image. Mixture models like GMM, HMRF, etc., suffer from high computational complexity because they execute a series of complex tasks in a sequential manner. Thus, the hardware implementation of such methods requires special attention.

Feature extraction and classification-based methods, at first, transform the image into a feature space and then classification is performed based on the set of features. For hardware realization, interpolation is often required during image transformation. In such a case, the hardware supporting interpolation operation could be a better choice. For classification methods like KNN, which are based on linear computation, parallel processing for hardware implementation is an uncomplicated task. As most of these methods involve iterations, global synchronization is required. As far as classification is concerned, ANN could be a better choice, because once the weights are learned, feedforward network can be used for hardware implementation to run in real time. Nowadays, CNNs are gaining more attention for brain tissue segmentation with efficient hardware implementation [121], [122].

In this paper, many evolutionary-based tissue segmentation methods are reported. These methods use global optimization techniques like EAs, which are very much responsive to parallelization. However, EAs are computationally expensive methods, which could decelerate real-time parallel processing [121], [122].

## V. Conclusion

Brain tissue segmentation is a topic of research in recent years. The accurate segmentation of brain tissue helps for disease diagnosis and treatment planning. However, it is not expected that the segmentation methods will replace experts in the diagnosis. They can be used to reduce the workload of the experts or can be used to provide a second opinion. The paper provides a framework for the recent algorithms used in brain tissue segmentation. The readers may gain an insight into state-of-the-art technology. The contributions of the paper are manifold. A quantitative analysis is carried out using various validation measures. This may help researchers for a comparison of segmentation methods. This survey also discusses the clinical usage and hardware implementation of different segmentation methods. This could particularly provide an idea to the researchers and clinicians about the method best suited for a desired application. We have presented a large set of performance indices and some public databases in order to compare and evaluate the performance of the existing brain tissue segmentation methods. Furthermore, these comparisons also consider each modality separately to select the best method. The paper focuses on recent challenges faced in handling brain tissue segmentation methods due to inherent problems in the imaging modalities. It is witnessed that incorporation of preprocessing steps like bias-field correction or IIH correction helps to improve the performance of the existing methods. The development of research software packages like SPM integrates such preprocessing steps. In addition, many modified methods are discussed. They perform well against bias-field or IIH. The merits and demerits of all existing segmentation algorithms are discussed. Some of the open problems are also addressed. This could provide researchers a future direction to improve brain tissue segmentation for accurate diagnosis.

## References


[1] M. M. Eapena, M. S. J. A. Ancelita, and G. Geetha, "Segmentation of tumors from ultrasound images with PAORGB," *Procedia Comput. Sci.*, vol. 50, pp. 663–668, 2015.

[2] L. Yang, O. Tuzel, P. Meer, and D. J. Foran, "Automatic image analysis of histopathology specimens using concave vertex graph," in *Proc. 11th Int. Conf. Med. Image Comput.Comput.-Assisted Intervention*, 2008, pp. 833–841.

[3] B. Foster, U. Bagci, A. Mansoor, Z. Xu, and D. J. Mollura, "A review on segmentation of positron emission tomography images," *Comput. Biol. Med.*, vol. 50, pp. 76–96, 2014.

[4] S. K. Adhikari, J. K. Sing, D. K. Basu, and M. Nasipuri, "Conditional spatial fuzzy C-means clustering algorithm for segmentation of MRI images," *Appl. Soft Comput.*, vol. 34, pp. 758–769, 2015.

[5] C. Chen, W. Xie, J. Franke, P. A. Grutzner, L. P. Nolte, and G. Zheng, "Automatic X-ray landmark detection and shape segmentation via data-driven joint estimation of image displacements," *Med. Image Anal.*, vol. 18, pp. 487–499, 2014.

[6] Y. Artan, A. Oto, and I. S. Yetik, "Cross-device automated prostate cancer localization with multiparametric MRI," *IEEE Trans. Image Process.*, vol. 12, pp. 5385–5394, Dec. 2013.

[7] S. Liao and D. Shen, "A feature-based learning framework for accurate prostate localization in CT images," *IEEE Trans. Image Process.*, vol. 21, no. 8, pp. 3546–3559, Aug. 2012.

[8] M. M. Fraz *et al.*, "An ensemble classification-based approach applied to retinal blood vessel segmentation," *IEEE Trans. Biomed. Eng.*, vol. 9, no. 9, pp. 2538–2548, Sep. 2012.

[9] L. Wen, X. Wang, Z. Wu, M. Zhou, and J. S. Jin, "A novel statistical cerebrovascular segmentation algorithm with particle swarm optimization," *Neurocomputing*, vol. 148, pp. 569–577, 2015.

[10] J. Ashburner and K. J. Friston, "Unified segmentation," *Neuroimage*, vol. 26, no. 3, pp. 839–851, 2005.

[11] K. Kazemi and N. Noorizadeh, "Quantitative comparison of SPM, FSL, and Brainsuite for brain MR image segmentation," *J. Biomed. Phys. Eng.*, vol. 4, no. 1, pp. 13–26, 2014.

[12] D. Mandal, A. Chatterjee, and M. Maitra, "Robust medical image segmentation using particle swarm optimization aided level set based global fitting energy active contour approach," *Eng. Appl. Artif. Intell.*, vol. 35, pp. 199–214, 2014.

[13] Y. Li, L. Jiao, R. Shang, and R. Stolkin, "Dynamic-context cooperative quantum-behaved particle swarm optimization based on multilevel thresholding applied to medical image segmentation," *Inf. Sci.*, vol. 294, pp. 408–422, 2015.

[14] H. Gao, W. B. Xu, J. Sun, and Y. Tang, "Multilevel thresholding for image segmentation through an improved quantum-behaved particle swarm algorithm," *IEEE Trans. Instrum. Meas.*, vol. 59, no. 4, pp. 934–946, Apr. 2010.

[15] M. Kass, A. Witkin, and D. Terzopoulos, "Snakes: Active contour models," *Int. J. Comput. Vis.*, vol. 1, no. 4, pp. 321–331, 1988.

[16] T. F. Chan and L. A. Vese, "Active contours without edges," *IEEE Trans. Image Process.*, vol. 10, no. 2, pp. 266–277, Feb. 2001.

[17] V. Caselles, R. Kimmel, and G. Sapiro, "Geodesic active contours," *Int. J. Comput. Vis.*, vol. 22, no. 1, pp. 61–79, 1997.

[18] M. Jacob, T. Blu, and M. Unser, "Efficient energies and algorithms for parametric snakes," *IEEE Trans. Image Process.*, vol. 13, no. 9, pp. 1231–1244, Sep. 2004.

[19] W. Kim and J. J. Lee, "Object tracking based on the modular active shape model," *Mechatronics*, vol. 15, no. 3, pp. 371–402, 2005.

[20] L. Jonasson *et al.*, "A level set method for segmentation of the thalamus and its nuclei in DT-MRI," *Signal Process.*, vol. 87, no. 2, pp. 309–321, 2007.

[21] R. H. Davies, C. J. Twining, T. F. Cootes, and C. J. Taylor, "Building 3-D statistical shape models by direct optimization," *IEEE Trans. Medical Imag.*, vol. 29, no. 4, pp. 961–981, Apr. 2010.

[22] M. Saadatmand-Tarzjan, "Self-affine snake for medical image segmentation," *Pattern Recognit. Lett.*, vol. 59, pp. 1–10, 2015.

[23] C. Li, X. Wang, S. Eberl, M. Fulham, Y. Yin, and D. D. Feng, "Supervised variational model with statistical inference and its application in medical image segmentation," *IEEE Trans. Biomed. Eng.*, vol. 62, no. 1, pp. 196–207, Jan. 2015.

[24] P. Mesejo, A. Valsecchi, L. Marrakchi-Kacem, S. Cagnoni, and S. Damas, "Biomedical image segmentation using geometric deformable models and metaheuristics," *Comput. Med. Imag. Graph.*, vol. 43, pp. 167–178, 2015.

[25] J. Cheng and S. W. Foo, "Dynamic directional gradient vector flow for snakes," *IEEE Trans. Image Process.*, vol. 15, no. 6, pp. 1563–1571, Jun. 2006.

[26] N. Jifeng, W. Chengke, L. Shigang, and Y. Shuqin, "NGVF: An improved external force field for active contour model," *Pattern Recognit. Lett.*, vol. 28, no. 1, pp. 58–63, 2007.

[27] C. Li, J. Liu, and M. D. Fox, "Segmentation of external force field for automatic initialization and splitting of snakes," *Pattern Recognit.*, vol. 38, no. 11, pp. 1947–1960, 2005.

[28] T. Liu, H. Zhou, F. Lin, Y. Pang, and J. Wu, "Improving image segmentation by gradient vector flow and mean shift," *Pattern Recognit. Lett.*, vol. 29, no. 1, pp. 90–95, 2008.

[29] N. Paragios, O. Mellina-Gottardo, and V. Ramesh, "Gradient vector flow fast geometric active contours," *IEEE Trans. Pattern Anal. Mach. Intell.*, vol. 26, no. 3, pp. 402–407, Mar. 2004.

[30] L. Qin, C. Zhu, Y. Zhao, H. Bai, and H. Tian, "Generalized gradient vector flow for snakes: New observations, analysis, and improvement," *IEEE Trans. Circuits Syst. Video Technol.*, vol. 23, no. 5, pp. 883–897, May 2013.

[31] Y. Wang, L. Liu, H. Zhang, Z. Cao, and S. Lu, "Image segmentation using active contours with normally biased GVF external force," *IEEE Signal Process. Lett.*, vol. 17, no. 10, pp. 875–878, Oct. 2010.

[32] C. Xu, A. Yezzi, and J. L. Prince, "On the relationship between parametric and geometric active contours," in *Proc. Conf. Rec. 34th Asilomar Conf. Signals, Syst. Comput.*, 2000, vol. 1, pp. 483–489.

[33] L. He *et al.*, "A comparative study of deformable contour methods on medical image segmentation," *Image Vis. Comput.*, vol. 26, no. 2, pp. 141–163, 2008.

[34] N. Paragios and R. Deriche, "Geodesic active regions: A new framework to deal with frame partition problems in computer vision," *J. Vis. Commun. Image Represent.*, vol. 13, no. 1, pp. 249–268, 2002.

[35] S. Ali and A. Madabhushi, "An integrated region-, boundary-, shape-based active contour for multiple object overlap resolution in histological imagery," *IEEE Trans. Med. Imag.*, vol. 31, no. 7, pp. 1448–1460, Jul. 2012.

[36] C. Pluempitiwiriyawej, J. M. Moura, Y. J. L. Wu, and C. Ho, "STACS: New active contour scheme for cardiac MR image segmentation," *IEEE Trans. Med. Imag.*, vol. 24, no. 5, pp. 593–603, May 2005.

[37] F. M. Sukno, S. Ordas, C. Butakoff, S. Cruz, and A. F. Frangi, "Active shape models with invariant optimal Features: Application to facial analysis," *IEEE Trans. Pattern Anal. Mach. Intell.*, vol. 29, no. 7, pp. 1105–1117, Jul. 2007.

[38] J. C. Nascimento and J. S. Marques, "Adaptive snakes using the EM algorithm," *IEEE Trans. Image Process.*, vol. 14, no. 11, pp. 1678–1686, Nov. 2005.

[39] G. Zhu, S. Zhang, Q. Zeng, and C. Wang, "Anisotropic virtual electric field for active contours," *Pattern Recognit. Lett.*, vol. 29, no. 11, pp. 1659–1666, 2008.

[40] M. A. Balafar, A. R. Ramli, M. I. Saripan, and S. Mashohor, "Review of brain MRI image segmentation methods," *Artif. Intell. Rev.*, vol. 33, no. 3, pp. 261–274, 2010.

[41] S. D. Olabarriaga and A. W. Smeulders, "Interaction in the segmentation of medical images: A survey," *Med. Image Anal.*, vol. 5, no. 2, pp. 127–142, 2001.

[42] A. Yezzi Jr., S. Kichenassamy, A. Kumar, P. Olver, and A. Tannenbaum, "A geometric snake model for segmentation of medical imagery," *IEEE Trans. Med. Imag.*, vol. 16, no. 2, pp. 199–209, Apr. 1997.

[43] L. A. Vese and T. F. Chan, "A multiphase level set framework for image segmentation using the Mumford and Shah model," *Int. J. Comput. Vis.*, vol. 50, no. 3, pp. 271–293, 2002.

[44] C. Li, X. Wang, S. Eberl, M. Fulham, and D. D. Feng, "A new energy framework with distribution descriptors for image segmentation," *IEEE Trans. Image Process.*, vol. 22, no. 9, pp. 3578–3590, Sep. 2013.

[45] C. Li *et al.*, "A likelihood and local constraint level set model for liver tumor segmentation from CT volumes," *IEEE Trans. Biomed. Eng.*, vol. 60, no. 10, pp. 2967–2977, Oct. 2013.

[46] Y. Boykov and V. Kolmogorov, "An experimental comparison of min-cut/max-flow algorithms for energy minimization in vision," *IEEE Trans. Pattern Anal. Mach. Intell.*, vol. 26, no. 9, pp. 1124–1137, Sep. 2004.

[47] L. Grady, "Random walks for image segmentation," *IEEE Trans. Pattern Anal. Mach. Intell.*, vol. 28, no. 11, pp. 1768–1783, Nov. 2006.

[48] R. Adams and L. Bischof, "Seeded region growing," *IEEE Trans. Pattern Anal. Mach. Intell.*, vol. 16, no. 6, pp. 641–647, Jun. 1994.

[49] A. Mehnert and P. Jackway, "An improved seeded region growing algorithm," *Pattern Recognit. Lett.*, vol. 18, no. 10, pp. 1065–1071, 1997.

[50] X. Lu, J. Wu, X. Ren, B. Zhang, and Y. Li, "The study and application of the improved region growing algorithm for liver segmentation," *Optik-Int. J. Light Electron Opt.*, vol. 125, no. 9, pp. 2142–2147, 2014.

[51] C. Li, R. Huang, Z. Ding, J. C. Gatenby, D. N. Metaxas, and J. C. Gore, "A level set method for image segmentation in the presence of intensity inhomogeneities with application to MRI," *IEEE Trans. Image Process.*, vol. 20, no. 7, pp. 2007–2016, 2011.

[52] C. Li, X. Wang, S. Eberl, M. Fulham, and D. D. Feng, "Robust model for segmenting images with/without intensity inhomogeneities," *IEEE Trans. Image Process.*, vol. 22, no. 8, pp. 3296–3309, Aug. 2013.

[53] D. Mumford and J. Shah, "Optimal approximations by piecewise smooth functions and associated variational problems," *Commun. Pure Appl. Math.*, vol. 42, no. 5, pp. 577–685, 1989.

[54] A. Tsai, A. Yezzi, Jr., and A. S. Willsky, "Curve evolution implementation of the Mumford-Shah functional for image segmentation, denoising, interpolation, and magnification," *IEEE Trans. Image Process.*, vol. 10, no. 8, pp. 1169–1186, Aug. 2001.

[55] M. E. Leventon, W. E. L. Grimson, and O. Faugeras, "Statistical shape influence in geodesic active contours," in *Proc. IEEE Comput. Vis. Pattern Recognit.*, 2000, pp. 316–323.

[56] C. Alvino, G. Unal, G. Slabaugh, B. Peny, and T. Fang, "Efficient segmentation based on eikonal and diffusion equations," *Int. J. Comput. Math.*, vol. 84, no. 9, pp. 1309–1324, 2007.

[57] A. Stadlbauer *et al.*, "Improved delineation of brain tumors: An automated method for segmentation based on pathologic changes of 1 H-MRSI metabolites in gliomas," *Neuroimage*, vol. 23, no. 2, pp. 454–461, 2004.

[58] K. J. Shanthi and K. M. Sasi, "Skull stripping and automatic segmentation of brain MRI using seed growth and threshold techniques," in *Proc. Conf. Intell. Adv. Syst.*, 2007, pp. 422–426.

[59] N. Gordillo, E. Montseny, and P. Sobrevilla, "State of the art survey on MRI brain tumor segmentation," *Magn. Reson. Imag.*, vol. 31, no. 8, pp. 1426–1438, 2013.

[60] J. N. Kapur, P. K. Sahoo, and A. K. Wong, "A new method for gray-level picture thresholding using the entropy of the histogram," *Comput. Vis., Graph. Image Process.*, vol. 29, no. 3, pp. 273–285, 1985.

[61] N. Otsu, "A threshold selection method from gray-level histograms," *Automatica*, vol. 11, pp. 23–27, 1975.

[62] M. Sezgin, "Survey over image thresholding techniques and quantitative performance evaluation," *J. Electron. Imag.*, vol. 13, no. 1, pp. 146–168, 2004.

[63] R. C. Gonzalez and R. E. Woods, *Digital Image Processing*. Englewood Cliffs, NJ, USA: Prentice-Hall, 2008.

[64] B. Akay, "A study on particle swarm optimization and artificial bee colony algorithms for multilevel thresholding," *Appl. Soft Comput.*, vol. 13, no. 6, pp. 3066–3091, 2013.

[65] P. D. Sathya and R. Kayalvizhi, "Optimal segmentation of brain MRI based on adaptive bacterial foraging algorithm," *Neurocomputing*, vol. 74, no. 14, pp. 2299–2313, 2011.

[66] P. D. Sathya and R. Kayalvizhi, "Optimal multilevel thresholding using bacterial foraging algorithm," *Expert Syst. Appl.*, vol. 38, no. 12, pp. 15549–15564, 2011.

[67] M. Maitra and A. Chatterjee, "A novel technique for multilevel optimal magnetic resonance brain image thresholding using bacterial foraging," *Measurement*, vol. 41, no. 10, pp. 1124–1134, 2008.

[68] S. Manikandan, K. Ramar, M. W. Iruthayarajan, and K. G. Srinivasagan, "Multilevel thresholding for segmentation of medical brain images using real coded genetic algorithm," *Measurement*, vol. 47, pp. 558–568, 2014.

[69] P. D. Sathya and R. Kayalvizhi, "Modified bacterial foraging algorithm based multilevel thresholding for image segmentation," *Eng. Appl. Artif. Intell.*, vol. 24, no. 4, pp. 595–615, 2011.

[70] C. Li, C. Xu, A. W. Anderson, and J. C. Gore, "MRI tissue classification and bias field estimation based on coherent local intensity clustering: A unified energy minimization framework," *Inf. Process. Med. Imag.*, vol. 21, pp. 288–299, 2009.

[71] Z. X. Ji, Q. Chen, Q. S. Sun, D. S. Xia, and P. A. Heng, "MR image segmentation and bias field estimation using coherent local and global intensity clustering," *Fuzzy Syst. Knowl. Discovery*, vol. 2, pp. 578–582, 2010.

[72] K. Sikka, N. Sinha, P. K. Singh, and A. K. Mishra, "A fully automated algorithm under modified FCM framework for improved brain MR image segmentation," *Magn. Reson. Imag.*, vol. 27, no. 7, pp. 994–1004, 2009.

[73] Z. X. Ji, Q. S. Sun, and D. S. A. Xia, "Modified possibilistic fuzzy c-means clustering algorithm for bias field estimation and segmentation of

brain MR image," *Comput. Med. Imag. Graph.*, vol. 35, no. 5, pp. 383–397, 2011.
[74] Z. Ji, Y. Xia, Q. Sun, Q. Chen, and D. Feng, "Adaptive scale fuzzy local Gaussian mixture model for brain MR image segmentation," *Neurocomputing*, vol. 134, pp. 60–69, 2014.
[75] K. S. Chuang, H. L. Tzeng, S. Chen, J. Wu, and T. J. Chen, "Fuzzy c-means clustering with spatial information for image segmentation," *Comput. Med. Imag. Graph.*, vol. 30, no. 1, pp. 9–15, 2006.
[76] N. A. Mohamed, M. N. Ahmed, and A. Farag, "Modified fuzzy c-mean in medical image segmentation," in *Proc. 20th Annu. Int. Conf. IEEE Eng. Med. Biol. Soc.*, 1998, pp. 1377–1380.
[77] L. Liao and T. S. Lin, "A fast spatial constrained fuzzy kernel clustering algorithm for MRI brain image segmentation," *Wavelet Anal. Pattern Recognit.*, vol. 1, pp. 82–87, 2007.
[78] D. Selvathi and R. Dhivya, "Segmentation of tissues in MR images using modified spatial fuzzy C means algorithm," in *Proc. Int. Conf. Signal Process. Imag. Process. Pattern Recognit*., 2013, pp. 136–140.
[79] C. Li, F. Li, C. Y. Kao, and C. Xu, "Image segmentation with simultaneous illumination and reflectance estimation: An energy minimization approach, in *Proc. IEEE 12th Int. Conf. Comput. Vis.*, 2009, pp. 702–708.
[80] Y. Chen, J. Zhang, and J. Macione, "An improved level set method for brain MR images segmentation and bias correction," *Comput. Med. Imag. Graph.*, vol. 33, no. 7, pp. 510–519, 2009.
[81] S. Krinidis and V. A. Chatzis, "Robust fuzzy local information C-means clustering algorithm," *IEEE Trans. Image Process.*, vol. 19, no. 5, pp. 1328–1337, May 2010.
[82] B. Caldairou, N. Passat, P. A. Habas, C. Studholme, and F. A. Rousseau, "Non-local fuzzy segmentation method: Application to brain MRI," *Pattern Recognit.*, vol. 44, no. 9, pp. 1916–1927, 2011.
[83] B. Caldairou, F. Rousseau, N. Passat, P. Habas, C. Studholme, and C. Heinrich, "A non-local fuzzy segmentation method: Application to brain MRI," in *Proc. Int. Conf. Comput. Anal. Imag. Patterns*, 2009, pp. 606–613.
[84] K. Mizutani and S. Miyamoto, "Possibilistic approach to kernel-based fuzzy c-means clustering with entropy regularization," in *Proc. 2nd Int. Conf. Model. Decis. Artif. Intell.*, 2005, pp. 144–155.
[85] T. Chaira, "A novel intuitionistic fuzzy C means clustering algorithm and its application to medical images," *Appl. Soft Comput.*, vol. 11, no. 2, pp. 1711–1717, 2011.
[86] F. U. Siddiqui, N. A. M. Isa, and A. Yahya, "Outlier rejection fuzzy c-means (ORFCM) algorithm for image segmentation," *Turkish J. Elect. Eng. Comput. Sci.*, vol. 21, no. 6, pp. 1801–1819, 2007.
[87] H. Greenspan, A. Ruf, and J. Goldberger, "Constrained Gaussian mixture model framework for automatic segmentation of MR brain images," *IEEE Trans. Med. Ima.*, vol. 25, no. 9, pp. 1233–1245, Sep. 2006.
[88] K. Blekas, A. Likas, N. P. Galatsanos, and I. E. Lagaris, "A spatially constrained mixture model for image segmentation," *IEEE Trans. Neural Netw.*, vol. 16, no. 2, pp. 494–498, Mar. 2005.
[89] M. A. Balafar, "Gaussian mixture model based segmentation methods for brain MRI images," *Artif. Intell. Rev.*, vol. 41, no. 3, pp. 429–439, 2014.
[90] J. Liu and H. Zhang, "Image segmentation using a local GMM in a variational framework," *J. Math. Imag. Vis.*, vol. 46, no. 2, pp. 161–176, 2013.
[91] A. N. Benaichouche, H. Oulhadj, and P. Siarry, "Improved spatial fuzzy c-means clustering for image segmentation using PSO initialization, mahalanobis distance and post-segmentation correction," *Digital Signal Process.*, vol. 23, no. 5, pp. 1390–1400, 2013.
[92] A. Mekhmoukh and K. Mokrani, "Improved Fuzzy C-Means based particle swarm optimization initialization and outlier rejection with level set methods for MR brain image segmentation," *Comput. Methods Prog. Biomed.*, vol. 122, no. 2, pp. 266–281, 2015.
[93] W. M. Wells, W. E. L. Grimson, R. Kikinis, and F. Jolesz, "Adaptive segmentation of MRI data," *IEEE Trans. Med. Imag.*, vol. 15, no. 4, pp. 429–442, Aug. 1996.
[94] R. Guillemaud and M. Brady, "Estimating the bias field of MR images," *Med. Imag.*, vol. 16, no. 3, pp. 238–251, 1997.
[95] K. V. Leemput, F. Maes, D. Vandermeulen, and P. Suetens, "Automated model-based bias field correction of MR images of the brain," *Med. Imag.*, vol. 18, no. 10, pp. 885–896, 1997.
[96] F. Dong and J. Peng, "Brain MR image segmentation based on local Gaussian mixture model and nonlocal spatial regularization," *J. Vis. Commun. Image Represent.*, vol. 25, no. 5, pp. 827–839, 2014.
[97] Z. Ji, J. Liu, G. Cao, Q. Sun, and Q. Chen, "Robust spatially constrained fuzzy c-means algorithm for brain MR image segmentation," *Pattern Recognit.*, vol. 47, no. 7, pp. 2454–2466, 2014.
[98] M. G. Sebastián, E. Fernández, M. Graña, and F. J. Torrealdea, "A parametric gradient descent MRI intensity inhomogeneity correction algorithm," *Pattern Recognit. Lett.*, vol. 28, no. 13, pp. 1657–1666, 2007.
[99] J. C. Rajapakse, J. N. Giedd, and J. L. Rapoport, "Statistical approach to segmentation of single-channel cerebral MR images," *Med. Imag.*, vol. 16, no. 2, pp. 176–186, 1997.
[100] Y. Zhang, M. Brady, and S. Smith, "Segmentation of brain MR images through a hidden Markov random field model and the expectation-maximization algorithm," *Med. Imag.*, vol. 20, no. 1, pp. 45–57, 2001.
[101] J. Besag, "On the statistical analysis of dirty pictures," *J. Roy. Statist. Soc. Ser. B (Methodological)*, vol. 48, pp. 259–302, 1986.
[102] B. Scherrer, M. Dojat, F. Forbes, and C. Garbay, "Agentification of Markov model-based segmentation: Application to magnetic resonance brain scans," *Artif. Intell. Med.*, vol. 46, no. 1, pp. 81–95, 2009.
[103] Z. Liang and S. Wang, "An EM approach to MAP solution of segmenting tissue mixtures: A numerical analysis," *IEEE Trans. Med. Imag.*, vol. 28, no. 2, pp. 297–310, Feb. 2009.
[104] J. Besag and C. Kooperberg, "On conditional and intrinsic autoregressions," *Biometrika*, vol. 82, no. 4, pp. 733–746, 1995.
[105] Z. Tu and S. C. Zhu, "Image segmentation by data-driven Markov chain Monte Carlo," *IEEE Trans. Pattern Anal. Mach. Intell.*, vol. 24, no. 5, pp. 657–673, May 2002.
[106] K. Kayabol, E. E. Kuruoğlu, and B. Sankur, "Bayesian separation of images modeled with MRFs using MCMC," *IEEE Trans. Image Process.*, vol. 18, no. 5, pp. 982–994, May 2009.
[107] J. Tohka, I. D. Dinov, D. W. Shattuck, and A. W. Toga, "Brain MRI tissue classification based on local Markov random fields," *Magn. Reson. Imag.*, vol. 28, no. 4, pp. 557–573, 2010.
[108] T. Zhang, Y. Xia, and D. D. Feng, "Hidden Markov random field model based brain MR image segmentation using clonal selection algorithm and Markov chain monte carlo method," *Biomed. Signal Process. Control*, vol. 12, pp. 10–18, 2014.
[109] T. Zhang, Y. Xia, and D. D. Feng, "An Evolutionary HMRF approach to brain MR image segmentation using clonal selection algorithm," *Biol. Med. Syst.*, vol. 8, no. 1, pp. 6–11, 2012.
[110] B. H. Ulutas and S. Kulturel-Konak, "A review of clonal selection algorithm and its applications," *Artif. Intell. Rev.*, vol. 36, no. 2, pp. 117–138, 2011.
[111] M. A. Jaffar, A. A. Mirza, and M. Mahmud, "MR imaging enhancement and segmentation of tumor using fuzzy curvelet," *Int. J. Phys. Sci.*, vol. 6, no. 31, pp. 7242–7246, 2011.
[112] N. Nabizadeh and M. Kubat, "Brain tumors detection and segmentation in MR images: Gabor wavelet vs. statistical features," *Comput. Elect. Eng.*, vol. 45, pp. 286–301, 2015.
[113] R. O. Duda, P. E. Hart, and D. G. Stork, *Pattern Classification*. Hoboken, NJ, USA: Wiley, 2012.
[114] P. Moeskops *et al.*, "Automatic segmentation of MR brain images with a convolutional neural network," *IEEE Trans. Med. Imag.*, vol. 35, no. 5, pp. 1252–1261, May 2016.
[115] M. Havaei *et al.*, "Brain tumor segmentation with deep neural networks," *Med. Image Anal.*, vol. 35, pp. 18–31, 2017.
[116] A. de Brebisson and M. Giovanni, "Deep neural networks for anatomical brain segmentation," in *Proc. IEEE Conf. Comput. Vis. Pattern Recognit. Workshops*, 2015, pp. 20–28.
[117] W. Zhang *et al*., "Deep convolutional neural networks for multi-modality isointense infant brain image segmentation," *NeuroImage*, vol. 108, pp. 214–224, 2015.
[118] G. D. Lorenzo, S. Francis, S. Narayanan, D. L. Arnold, and D. L. Collins, "Review of automatic segmentation methods of multiple sclerosis white matter lesions on conventional magnetic resonance imaging," *Med. Image Anal.*, vol. 17, pp. 1–18, 2013.
[119] MRBrainS. "Evaluation framework for MRBrain image Segmentation," 2013. [Online]. Available: http://mrbrains13.isi.uu.nl/results.php
[120] E. S. A. El-Dahshan, H. M. Mohsen, K. Revett, and A. B. M. Salem, "Computer-aided diagnosis of human brain tumor through MRI: A survey and a new algorithm," *Expert Syst. Appl.*, vol. 41, no. 11, pp. 5526–5545, 2014.
[121] A. Eklund, P. Dufort, D. Forsberg, and S. M. LaConte, "Medical image processing on the GPU–Past, present and future," *Med. Image Anal.*, vol. 17, no. 8, pp. 1073–1094, 2013.
[122] E. Smistad, T. L. Falch, M. Bozorgi, A. C. Elster, and F. Lindseth, "Medical image segmentation on GPUs–A comprehensive review," *Med. Image Anal.*, vol. 20, no. 1, pp. 1–18, 2015.

Authors' photographs and biographies not available at the time of publication.